Hierarchical thermoplastic biocomposites reinforced with flax fibres modified by xyloglucan and cellulose nanocrystals

Estelle Doineau, Guillaume Coqueugniot, Monica Francesca Pucci, A. S. Caro-Bretelle, Bernard Cathala, Jean-Charles Bénézet, Julien Bras, Nicolas Le Moigne

Hierarchical thermoplastic biocomposites reinforced with flax fibres modified by xyloglucan and cellulose nanocrystals

Estelle Doineau [a,b,c,*], Guillaume Coqueugniot [b], Monica Francesca Pucci [d], Anne-Sophie Caro [d], Bernard Cathala [c], Jean-Charles Bénézet [a], Julien Bras [b,e], Nicolas Le Moigne [a,*]

[a] Polymers Composites and Hybrids (PCH), IMT Mines Ales, Ales, France[1]
[b] Univ. Grenoble Alpes, CNRS, Grenoble INP (Institute of Engineering Univ. Grenoble Alpes), LGP2, F-38000, Grenoble, France[1]
[c] INRAE, UR BIA, F-44316, Nantes, France[1]
[d] LMGC, IMT Mines Ales, Univ Montpellier, CNRS, Ales, France[1]
[e] Nestle Research Center, CH – 1000, Lausanne, Switzerland

A B S T R A C T

This work is focused on the modification of the interphase zone in short flax fibres / polypropylene (PP) com-posites by a bio-inspired modification of fibres called "nanostructuration" that uses the adsorption of biomass by- products, i.e. cellulose nanocrystals (CNC) and xyloglucan (XG), to create hierarchical flax fibres. The wettability and interfacial adhesion study reveals a strong decrease in the polar character of CNC modified flax fibres, hence increasing the work of adhesion with PP. Moreover, combining XG/CNC modified interphases with MAPP coupling agent enhances the ultimate mechanical properties of biocomposites with higher tensile strength and work of rupture, and modifies failure mechanisms as revealed by *in situ* micro-mechanical tensile SEM experi-ments. Bio-based hierarchical composites inspired by naturally occurring nanostructures open a new path for the development of sustainable composites with enhanced structural properties.

Keywords:
Flax fibres
Xyloglucan
Cellulose nanocrystals
Hierarchical interphase

1. Introduction

Considering the current environmental concerns towards the creation of eco-friendly materials that are entirely or partially biobased, the use of natural fibres as reinforcements in biocomposites in sectors like automotive, building and construction or sports is a great opportunity and has been the subject of various recent scientific reviews (Bourmaud, Shah, Placet, & Baley, 2018; Lau, Hung, Zhu, & Hui, 2018; Mohanty, Pin, & Misra, 2018; Sanjay et al., 2018; Pickering, Aruan Efendy, & Le, 2016; Yan, Chouw, & Jayaraman, 2014; Müssig, 2010). Natural fibres have many advantages compared to synthetic fibres, such as their renewability, biodegradability, wide availability and low cost associated with low density and high specific mechanical properties. However, the implementation of these materials in industrial applications is limited by the low thermal and dimensional stability of natural fibres, especially in humid conditions, as well as poor interfacial adhesion with several polymer matrices (Baley, Le Duigou, Bourmaud, & Davies, 2012; Garat, Le Moigne, Corn, Beaugrand, & Bergeret, 2020; Khaldi, Bouziane, Vivet, & Bougherara, 2019; Le Duigou, Bourmaud, Balnois, Davies, & Baley, 2012; Le Duigou et al., 2017). The fibre / matrix interface plays a key role in stress transfer within biocomposite materials and their resulting mechanical performance. The main difficulty comes from the polar and hydrophilic character of lignocellulosic fibres considering their global biochemical composition and surface chemistry, whereas the thermoplastic polymer matrices often display a hydrophobic and apolar character (Bismarck et al., 2002; Faruk, Bledzki, Fink, & Sain., 2012).

To tackle these fibre / matrix compatibility issues, a wide panel of chemical and physical modifications of natural fibre surfaces have been reported in the literature (Le Moigne, Otazaghine, Corn, Angellier-Coussy, & Bergeret, 2018; Lee, Delille, & Bismarck, 2011; Mohanty, Misra, & Drzal, 2001; Zafeiropoulos, 2011). For example, coupling agents such as MAPP or MAPE were used in biocomposites to create chemical bonds between natural fibres and polyolefins (Elsabbagh, Steuernagel, & Ziegmann., 2009; Lu, 2000; Mohanty, Nayak, Verma, & Tripathy., 2016; Park, Quang, Hwang, & Lawrence DeVries, 2006). Another strategy mostly used in synthetic composites consists of deposition of nanoparticles on fibre surfaces. This concept is directly inspired from naturally occurring composites such as bones, shells and

* Corresponding authors at: Polymers Composites and Hybrids (PCH), IMT Mines Ales, Ales, France.
E-mail addresses: doineau.estelle@orange.fr (E. Doineau), nicolas.le-moigne@mines-ales.fr (N. Le Moigne).
[1] Members of the European Polysaccharide Network of Excellence (EPNOE), https://epnoe.eu/.

teeth which show hierarchical nanoscaled structures with amazing mechanical behaviour (Gao, Ji, Jager, Arzt, & Fratzl, 2003; Gupta et al., 2006). The design of bio-inspired hierarchical composites involves for instance the development of hierarchical fibres by the deposition of carbon nanotubes, ZnO nanowires, nanoclays, cellulose nanocrystals onto carbon, glass or natural fibres (Asadi, Miller, Singh, Moon, & Kalaitzidou, 2017; Karger-Kocsis, Mahmood, & Pegoretti, 2020; Asadi, Miller, Sultana, Moon, & Kalaitzidou, 2016; Karger-Kocsis, Mahmood, & Pegoretti, 2015; Saba, Jawaid, & Asim., 2016; Sharma et al., 2014; Yang, Han, Nie, & Wang., 2020). The purpose is to take advantage of nano-objects at the interphase to achieve local reinforcement and enhance the mechanical interlocking between fibres and matrix (Daniel Wagner, 2002; Hughes, Morley, & Jackson., 1980).

Some studies focused on fully bio-based nanostructuration of natural fibres with the use of bacterial cellulose (BC), cellulose nanofibrils (CNF) or cellulose nanocrystals (CNC). The deposition of BC and CNF on sisal, hemp and flax fibre surfaces was investigated in several studies (Blaker, Lee, & Bismarck, 2011; Fortea-Verdejo, Lee, Zimmermann, & Bismarck, 2016; Juntaro, Pommet, Mantalaris, Shaffer, & Bismarck, 2007; Juntaro et al., 2008; Lee, Bharadia, Blaker, & Bismarck, 2012; Pommet et al., 2008). Lee et al. successfully created "hairy" coated sisal fibres via their dipping in a slurry of BC for the reinforcement of PLA based biocomposites (Lee et al., 2012). The results were promising with a strong increase of the specific surface area up to 800 % compared to neat sisal fibres. Moreover, the storage modulus of the PLA / BC coated sisal fibres based biocomposite was increased by roughly 20 % compared to PLA / neat sisal fibres. However, the modification of natural fibres by bacterial cellulose requires specific conditions to control the fermentation bioprocess, i.e. the culture medium, pH, temperature and especially the incubation time that can last for several days. Very few papers deal with the deposition of CNC on natural fibre surfaces. Dai and Fan worked on the deposition of CNC on hemp fibres and its effects on the fibre properties and adsorption of polyester resin, but did not study the mechanical performance of composites (Dai & Fan, 2013). Ghasemi et al. studied the process of CNF and CNC deposition on hemp and flax yarns and the resulting mechanical properties of the fibres, but did not prepare any composites with the treated yarns (Ghasemi, Tajvidi, Bousfield, & Gardner, 2018). The only works dealing with the use of CNC as interfacial modifier in biocomposites were conducted by Hajlane et al. (Hajlane, Kaddami, & Joffe, 2017; Hajlane, Joffe, & Kaddami, 2018). The authors worked on the adsorption of CNC on regenerated cellulose fibre surfaces. They showed that fibres treated with CNC adsorbed two times less water than untreated fibres at RH of 64 % and exhibited an increase in the interfacial shear strength (IFSS) with an epoxy resin matrix.

In this context, the goal of this work is to modify flax fibre surfaces by nanostructuration with CNC so as to reinforce apolar polymer matrices. It has been shown in literature that the strength of the interfacial adhesion is mainly governed by the polymer surface tension, the fibre surface free energy and also to the surface chemistry and topography of the fibres (Le Duigou, Kervoelen, Le Grand, Nardin, & Baley, 2014; Liotier et al., 2019). Nanostructuration with CNCs appears interesting as they display a high specific surface area of 150–800 m^2/g and a high Young's modulus of 150 GPa ± 50 GPa (Dufresne, 2017; Foster et al., 2018; Klemm et al., 2011; Moon, Martini, Nairn, Simonsen, & Youngblood, 2011). Moreover, Khoshkava and Kamal found a total surface free energy of CNC $\gamma_{CNC} = 68.9\ mJ/m^2$, being characterized by a predominant dispersive component, i.e. $\gamma^d_{CNC} = 40.9\ mJ/m^2$ against $\gamma^p_{CNC} = 28.0\ mJ/m^2$ for the polar component (Khoshkava & Kamal, 2013), due to its highly crystalline and (almost pure) cellulosic structure. This characteristic could be very interesting to enhance the interfacial adhesion with apolar polymer matrices such as polypropylene (PP). Moreover, our previous work that focused on the adsorption mechanisms of CNC and xyloglucan (XG) on flax fibre surfaces highlighted the creation of an extensible network XG/CNC on the surface of fibres (Doineau et al., 2020). Indeed, XG displays strong affinities with cellulosic surfaces via hydrogen bonds and van der Waals interactions, which stimulated researchers to create green materials such as XG/cellulose aerogels and films (Cerclier et al., 2011, 2013; Jaafar et al., 2020; Jean, Heux, Dubreuil, Chambat, & Cousin, 2009; Sehaqui, Zhou, & Berglund, 2011). We hypothesize that the deposition of such XG/CNC complex on natural fibres could be of interest for composite applications by providing an expended interphase region with modified interfacial adhesion and enhanced mechanical performance.

This work will focus on the surface modification of short flax fibres by the adsorption of cellulose nanocrystals (CNC) and xyloglucan (XG), and the resulting interfacial adhesion and mechanical behaviour of PP / flax biocomposites prepared by extrusion and injection moulding. The coupling agent maleic anhydride grafted polypropylene (MAPP) was also incorporated in some biocomposites to provide chemical interactions and improve the compatibility between the PP matrix and (modified) flax fibres (Mohanty et al., 2016; Park et al., 2006). Wettability tests on CNC and XG/CNC modified flax fibres, and mechanical tests on biocomposites at macro- and microscopic length scales were performed. In addition, possible changes in microstructure such as crystallinity, fibre size and shape distribution, which could also influence the final mechanical performances of the materials, were analysed.

2. Materials and methods

2.1. Materials

Flax fibre bundles of average length 2.24 mm and width 110 μm (initial aspect ratio around 20) were supplied by Fibres Recherche Développement (Troyes, France). Their biochemical composition was characterized according to van Soest method (standards NF EN ISO 13,906 and NF V18-122): cellulose (79.7 ± 1.7 wt%), hemicelluloses (5.6 ± 1.0 wt%), lignin (2.8 ± 0.3 wt%), solubles (11.2 ± 0.5 wt%) and ash (0.7 ± 0.3 wt%). Polypropylene (PP), grade PPH 9020, homopolymer, was purchased from Total Petrochemicals (Melting point =165 °C; Density 0.905 g/cm^3). Maleic anhydride-grafted polypropylene (MAPP) OREVAC CA100 was purchased from Arkema (MA content = 1%; Melting point =167 °C). Cellulose nanocrystals (CNC) were obtained by acid hydrolysis of wood pulp and provided in spray-dried powder by CelluForce (Quebec, Canada). CNC lateral dimensions: 2−5 nm; CNC length: 50−110 nm; CNC surface charge density: 0.023 mmol/g; Crystalline fraction: 0.88. Xyloglucan (XG) Glyloid 6 C was obtained from tamarind seed gum and purchased from DSP Gokyo Food & Chemical. M_w = 840 000 g/mol; M_w/M_n = 1.24; R_g 72 nm. Monosaccharide composition: glucose 50.7 %; xylose: 31.7 %; galactose 16.0 %; arabinose 1.6 %.

2.2. Flax fibres modification by CNC and XG

Cellulose nanocrystals (CNC) and xyloglucan (XG) were adsorbed on short flax fibre bundles. At first, flax fibres were modified only with CNC. A CNC suspension was prepared under stirring during 2 h (10 g of CNC in 1 L deionized water) followed by sonication (cycle 5; amplitude 50 %; 2 × 1 min) to break residual CNC agglomerates. Then, 10 g of flax fibres were added to the CNC suspension and gently stirred during 5 min to obtain a good dispersion of flax fibres within the suspension. The resulting mixture was stored at 4 °C during 24 h. The CNC modified fibres were then filtered with a Büchner system and dried at 105 °C during 2 h.

The same procedure was followed for the modification of flax fibres with both XG and CNC. In this case, XG was firstly adsorbed onto flax fibres as follows: XG suspension was prepared, i.e. 10 g of XG added gradually in 1 L deionized water with a vortex mixer, at 50–60 °C during few hours. Then, 10 g of flax fibres were added in the XG solution and gently stirred during 5 min to obtain a good dispersion of flax fibres within the solution. The resulting mixture was stored at 4 °C during 24 h.

The XG modified fibres were then filtered with a Büchner system and dried at 105 °C during 2 h. These fibres were then modified with CNC following the procedure described above.

The resulting CNC and XG/CNC modified flax fibres, named flax_CNC and flax_XG/CNC respectively, were stored in a conditioning room at 23 °C and 50 % relative humidity. Note that more details about sorption isotherms and localization of XG and CNC on flax fibres can be found in our previous work (Doineau et al., 2020). Based on this study, the adsorbed amounts of XG or CNC onto flax fibre surfaces were estimated around 2 wt% (20 mg / g_{fibre}).

2.3. Surface free energy of flax fibres

As flax fibre bundles are dispersed and individualized in the matrix during composite processing, elementary flax fibres extracted from an unidirectional flax woven fabric 300 g / m^2 (FRD, France) were used for these experiments, and modified with CNC and XG/CNC following the same procedure described in section 2.2. The tensiometer K100SF (Krüss, GmbH) was used to perform wettability tests in different reference liquids following the Wilhelmy method (Eq. 1):

$$F = m.g = \gamma_L^{tot}.p.\cos\theta_e \quad (1)$$

With F the capillary force (mN) measured by the tensiometer when a single fibre is immersed in the test liquid, m (g) corresponding to the mass of the liquid meniscus formed around the immersed elementary fibre, γ_L^{tot} (mN/m) the liquid surface tension, p (µm) the fibre wetted length or perimeter and θ_e (°) the static advancing contact angle between the fibre and the liquid (Pucci et al., 2017). Due to the heterogeneity of elementary flax fibre diameters, the perimeter p was determined beforehand for each tested fibre by using n-hexane (Sodipro) which has a surface tension γ_L^{tot} = 18.4 mN/m, and is a totally wetting liquid, implying that $\cos\theta_e = 1$. Then, the tested fibres were dried (16 h, 60 °C) to remove any residual n-hexane before being tested in the two other reference liquids, i.e. water, diiodomethane (Sodipro). The contact angle between the elementary flax fibre and the reference liquids was determined as follows. The elementary flax fibres (modified or not) were dipped at a velocity of 1 mm/min in a vessel containing the test liquid. The vessel was approached manually close to the fibre extremity and a fixed depth immersion was set in order to have at least 3–4 mm immersion depth. During immersion (advancing mode), the mass m is measured to obtain the contact angle. When immersion is completed, the fibre is maintained in contact with the liquid in a static position during 60 s in order to reach an "equilibrium state". At equilibrium, the capillary force is measured and the corresponding static advancing contact angle θ_e is derived from the Eq. (1). Then, the fibre is withdrawn from the liquid (receding mode). Tensiometric tests were carried out on eight samples for each type of fibre, i.e. raw flax fibres, CNC and XG/CNC modified flax fibres. Results were reproducible and gave low standard deviations.

2.4. Biocomposites processing

Blends of PP or PP / MAPP loaded at 5, 20 and 30 wt% of raw, flax_CNC or flax_XG/CNC modified fibres were compounded in a co-rotating twin-screw DSM Micro 15 extruder. The amount of MAPP was fixed at a ratio of flax fibres / MAPP (w / w) = 10. This ratio was shown to give the most efficient compatibilization between PP matrix and flax fibres (Snijder & Bos, 2000). Compositions of the different biocomposites are detailed in Table 1.

Flax fibres were dried before compounding in an oven at 80 °C during 2 h. The PP matrix or PP / MAPP pre-mix were introduced simultaneously with raw and modified flax fibres in the mixing chamber. Processing temperature was roughly 185–190 °C (setpoint temperature) with a screw speed of 50 rpm and a processing time of 10 min. The resulting biocomposite compounds were collected and pelletized to around 4 mm diameter. Then, pelletized compounds were shaped by injection moulding with a HAAKE Minijet Inject press (Thermofisher), into dumbbells type 5A specimens (ISO 157-2) for the measurement of mechanical properties. Injection conditions were T_{inject} =180 °C, P_{inject} =650 bar during 15 s and T_{mold} =50 °C. Biocomposite specimens were stored in a conditioning room at 23 °C and 50 % relative humidity during at least 48 h, prior to mechanical tests.

Table 1
Composition of the different extruded and injected biocomposites.

Designations	Fibre content (wt%)		
	5 %	20 %	30 %
	Matrix composition (wt%)		
PP_flax	95 % PP	80 % PP	70 % PP
PP_flax_CNC			
PP_MAPP_flax	94.5 % PP +	78 % PP +	67 % PP +
PP_MAPP_flax_CNC	0.5 % MAPP	2 % MAPP	3 % MAPP
PP_MAPP_flax_XG/CNC	/	78 % PP + 2 % MAPP	/

2.5. Differential scanning calorimetry (DSC)

Differential Scanning Calorimetry (DSC) tests were carried out using Perkin-Elmer Pyris Diamond DSC, equipped with an Intracooler II using nitrogen as purge gas. Samples of 10 mg were cut from the injection moulded specimens and placed in aluminium pans. The thermal cycle was a first heating from 10 to 200 °C, then cooling down to 10 °C and a second heating up to 200 °C with heating/cooling rates of 10 °C/min and holding times of 2 min between each step. Two samples were tested per material. Results were highly reproducible and gave low standard deviations. Melting enthalpies ΔH_m (J/g) were determined between 143 and 175 °C on the first heating ramp. The degree of crystallinity X_c (%) was calculated according to the following Eq. (2):

$$X_c = \left(\frac{|\Delta H_m|}{\chi_{matrix} \times |\Delta H_m^0|} \right) \times 100 \quad (2)$$

Where ΔH_m° is the melting enthalpy of 100 % crystalline PP (207 J/g) (Blaine, 2002), ΔH_m is the melting enthalpy of the sample (J/g) and χ_{matrix} is the weight fraction of PP or PP / MAPP within the sample.

2.6. Microstructural analysis by SEM

Microstructural analysis of the biocomposites was conducted on tensile specimens polished in the central zone down to 300 µm below the surface, ensuring that samples were observed in the shell/core zone (Abdennadher, 2015; Bay & Tucker, 1992). These polished samples were observed by Scanning Electron Microscopy SEM (FEI Quanta 200) and cartographies of 4 mm x 4 mm consisting of 16 SEM images were built using the software Aztec® (Oxford Instruments). All the SEM observations were made on samples sputter coated with carbon using a BALZERS CED 030 in order to avoid any degradation. Micrographs were obtained under high vacuum at acceleration voltage 12.5 keV. Based on cartographies, fibre size and shape distributions were analysed with the software AphelionTM V.4.3.2 (ADCIS and Amerinex Applied Imaging Inc.), which automatically detects the outlines of the fibres present on the pictures. Fibre length (L) and width (W) were determined based on the maximum and minimum Feret's diameters with roughly 1300 fibres per cartography. The fibre shape is defined by its aspect ratio (L / W), i.e. the ratio between the maximum and the minimum Feret's diameter. Overlapped fibres were excluded from the counts. Because of the picture resolution (0.67 µm/pixel), the particles with the maximum size smaller than 335 μm^2 (corresponding to cell wall fragments) were not considered in the fibre size and shape distributions. The number weighted and surface weighted fibre aspect ratio (L/W) distributions were established

(Le Moigne, van Den Oever, & Budtova, 2011).

2.7. Tensile properties

Tensile properties of the biocomposites were measured with a Zwick TH 010 testing machine equipped with an extensometer Zwick "clip-on" for the determination of the Young's modulus (ISO 527 standard). The displacement speed of the crosshead was 1 mm/min for the determination of the Young's modulus and 10 mm/min for the determination of the ultimate tensile properties (ultimate strength, elongation at break and work of rupture). Five samples per material were tested and the standard deviations are given for each of the mechanical properties.

2.8. In situ micro-mechanical tensile SEM experiments

The SEM was equipped with a tensile stage (DEBEN microtest, maximum load 5 kN) to analyse interfacial failure mechanisms. Direct observations of the crack propagation were conducted at a displacement speed of 0.1 mm/min on notched specimens with dimensions of 20 mm × 5 mm × 2 mm and a notch of 1 mm depth and 45 ± 1° opening. Before testing, notched samples were polished to remove the 100 μm thick polymer layer from the surface and better observe failure mechanisms between the fibres and the matrix. Experiments were performed twice per material.

3. Results and discussions

3.1. Surface free energy of flax fibres and work of adhesion

Total surface free energy γ_s^{tot} of elementary flax fibre and its polar and dispersive components γ_s^p and γ_s^d (mJ/m^2) were determined by the Owens, Wendt, Rabel and Kaelble (OWRK) approach (Owens & Wendt, 1969) knowing the respective polar and dispersive surface tensions of the testing liquids γ_L^p and γ_L^d (mN/m), Eq. (3):

$$\frac{\gamma_L^{tot}(1+\cos\theta_e)}{2\sqrt{\gamma_L^d}} = \sqrt{\gamma_S^p} \times \sqrt{\frac{\gamma_L^p}{\gamma_L^d}} + \sqrt{\gamma_S^d} \quad (3)$$

Polar and dispersive surface tension values of water (γ_L^p = 51.0 mN/m; γ_L^d = 21.8 mN/m), *n*-hexane (γ_L^p = 0 mN/m; γ_L^d = 18.4 mN/m), diiodomethane (γ_L^p = 2.3 mN/m; γ_L^d = 48.5 mN/m) have been used. The resulting surface free energy and its dispersive and polar component values are reported in Table 2 for non-treated and treated flax fibres. It was verified beforehand that the wetted length did not change after immersion in liquids, meaning that fibre swelling did not occur, and hence this phenomenon was not considered for surface energy determination (Pucci et al., 2017). Raw flax fibres have a total surface free energy of 34.3 ± 3.2 mJ/m^2 with polar and dispersive components of 18.2 ± 3.0 mJ/m^2 and 16.1 ± 0.2 mJ/m^2, respectively. First, the presence of cellulose nanocrystals (CNC) at the surface of flax fibres decreases their total surface free energy to 30.9 ± 1.9 mJ/m^2. Its polar component is greatly decreased from 18.2 ± 3.0 mJ/m^2 to 12.9 ± 0.8 mJ/m^2 while its dispersive component is slightly increased from 16.1 ± 0.2 mJ/m^2 to 18.0 ± 1.1 mJ/m^2.

Table 2
Surface free energies (with their polar and dispersive components) for non-treated and treated flax fibres at 20 °C, and for PP and MAPP matrices at 20 °C (taken from Fuentes et al., 2018) and 190 °C (calculated from literature data obtained between 20 °C and 220 °C).

Temperature 20 °C	γ_S^p (mJ/m²)	γ_S^d (mJ/m²)	γ_S^{tot} (mJ/m²)
PP (Fuentes et al., 2018)	0.1	30.5	30.6
MAPP (Fuentes et al., 2018)	0.3	31.8	32.1
Flax	18.2 ± 3.0	16.1 ± 0.2	34.3 ± 3.2
Flax_CNC	12.9 ± 0.8	18.0 ± 1.1	30.9 ± 1.9
Flax_XG/CNC	17.5 ± 3.8	16.8 ± 0.4	34.4 ± 4.2
Temperature 190 °C	γ_L^p (mN/m)	γ_L^d (mN/m)	γ_L^{tot} (mN/m)
PP *	0.1	21.1	21.2
MAPP *	0.2	22.0	22.2

* calculated from Fuentes et al. (2018); Khoshkava and Kamal (2013); Kwok et al. (1998); Schonhorn and Sharpe (1965); Tran et al. (2013).

As explained in the introduction section, CNC displays predominantly dispersive character due to its crystalline and almost pure cellulosic structure. This characteristic may explain the increased dispersive character of CNC modified flax fibres. Topographical changes at the flax fibre surface due to nanostructuration with CNC might also play a role. In fact, the wettability of a surface is governed by its physico-chemical interactions with test liquids but also by its surface morphology and characteristics including roughness and specific surface area (Li et al., 2002). Qian et al. obtained the same trend via the grafting of carbon nanotubes on a carbon fibre surface with a pronounced decrease of the total surface energy of the carbon fibre from 54.6 ± 1.4 mJ/m^2 to 38.8 ± 2.4 mJ/m^2 (Qian, Bismarck, Greenhalgh, Kalinka, & Shaffer, 2008). The polar part decreased strongly from 29.7 ± 1.0 mJ/m^2 to 1.0 ± 0.6 mJ/m^2 while an increase of the dispersive part from 24.9 ± 0.4 mJ/m^2 to 37.8 ± 1.9 mJ/m^2 was observed.

For the XG/CNC modified flax fibres, no changes were observed, with total surface free energy and polar and dispersive components similar to the raw flax fibres. Hemicelluloses such as xyloglucan have a pronounced polar character (Pirich et al., 2015) and could counterbalance the dispersive effect of CNC on the fibre surface free energy.

Based on the respective surface free energy of flax fibres and surface tension of the molten matrices, i.e. PP or MAPP, it is possible to predict the adhesion strength at the fibre / matrix interface. The work of adhesion (W_A) greatly influences the wettability of the fibres towards the matrix during processing and plays a role in the interfacial adhesion within the final biocomposite. The higher the W_A, the better would be the wettability and the quality of adhesion between fibres and matrix. The work of adhesion W_A (mJ/m^2) was calculated with Eq. (4) derived from the OWRK approach (Owens & Wendt, 1969) based on the geometric mean of dispersive and polar components of the liquid surface tension and solid surface free energy:

$$W_A = 2 \times \left[\sqrt{\gamma_S^d \times \gamma_L^d} + \sqrt{\gamma_S^p \times \gamma_L^p}\right] \quad (4)$$

And with the Eq. (5) derived from the Wu approach (Wu, 1971) based on the harmonic mean of dispersive and polar components of the liquid surface tension and solid surface free energy:

$$W_A = 4 \times \left(\frac{\gamma_L^d \cdot \gamma_S^d}{\gamma_L^d + \gamma_S^d} + \frac{\gamma_L^p \cdot \gamma_S^p}{\gamma_L^p + \gamma_S^p}\right) \quad (5)$$

Surface energy / tension values of PP at various temperatures measured either by the sessile drop (low temperature) or the pendant drop (high temperature) techniques (Kwok, Cheung, Park, & Neumann, 1998; Tran, Fuentes, Dupont-Gillain, Van Vuure, & Verpoest, 2013, Fuentes et al., 2018, Khoshkava & Kamal, 2013; Schonhorn & Sharpe, 1965) have been used to determine the surface tension of PP at a temperature of 190 °C, corresponding to the processing conditions used in the micro-compounder. We considered that the evolution of the surface tension and polarity of PP and MAPP is linear over the temperature range 20–220 °C, i.e. a constant polarity ratio $\gamma_L^p/\gamma_L^{tot}$ (0.003 for PP and 0.01 for MAPP determined at 20 °C from Fuentes et al., 2018) and a constant ratio $\gamma_{PP}^{tot}/\gamma_{MAPP}^{tot}$ (0.953 determined at 20 °C from Fuentes et al., 2018). On this basis, we calculated the surface tension and its polar and dispersive components for PP and MAPP at 190 °C (see Table 2). Based on our calculation, the increase in temperature decreases the total surface free energy of PP and MAPP with a surface energy thermal coefficient k = - 0.0495 mJ / m^2 °C. Note that the variations of polar and dispersive components of these polymers as a function of temperature are not well known but considering the quasi-dispersive character of

polyolefin matrices, we expect that variations should be limited.

The work of adhesion W_A between flax fibres and PP or MAPP was thus determined according to Eqs. (4) and (5), and considering the surface tension of PP or MAPP in the molten state at 190 °C and the surface energies of raw flax and flax_CNC or flax_XG/CNC fibres determined by tensiometric tests on single fibres at 20 °C given in Table 2. Besides, the values of W_A determined for flax fibres / MAPP suppose a complete migration of MAPP to the fibre / PP matrix interface during the compounding process. The resulting works of adhesion for the different systems are compared in Fig. 1.

As detailed in the materials and methods, two different approaches were used to calculate W_A (mJ/m^2), i.e. the OWRK approach (Eq. 4) and the Wu approach (Eq. 5). OWRK approach is widely used in the literature dealing with interfacial adhesion in composites. However, Wu assumed that the harmonic mean approach gives more consistent results for low energy system interactions, the geometric mean approach being more suitable to high energy systems like adhesives on metals (Wu, 1971). As can be seen in Fig. 1, the Wu approach gives lower work of adhesion for both PP and MAPP matrices compared to OWRK approach. Taking the example of PP matrix, W_A varies from 36.9 ± 0.3 to 39.3 ± 1.3 mJ/m^2 (Wu) against 39.6 ± 0.5 mJ/m^2 to 41.2 ± 1.3 mJ/m^2 (OWRK) for the different flax fibres (raw, flax_CNC or flax_XG/CNC).

Firstly, it is noticeable that the work of adhesion is slightly increased with MAPP whatever the calculation approach and fibre treatment. This suggests a better adhesion and wettability of non-treated and treated flax fibres in the presence of MAPP. This is related to the highest surface tension and polarity of MAPP (versus PP) brought by maleic anhydride functional groups grafted on PP chains (Berzin et al., 2020). Secondly, a moderate increase of the work of adhesion between CNC treated flax fibres and PP is observed, i.e. from 39.6 ± 0.5 mJ/m^2 to 41.2 ± 1.3 mJ/m^2 (OWRK) and 36.9 ± 0.3 mJ/m^2 to 39.3 ± 1.3 mJ/m^2 (Wu). Similar trends are also observed for CNC treated flax fibres and MAPP, i.e. from 41.5 ± 0.6 mJ/m^2 to 43.0 ± 1.3 mJ/m^2 (OWRK) and 38.0 ± 0.3 mJ/m^2 to 40.4 ± 1.4 mJ/m^2 (Wu). It thus appears that the increase dispersive character of CNC treated fibres promotes the adhesion with mostly apolar polymer matrices such as PP and MAPP. In contrast, the XG/CNC treated fibres only bring slight improvement of the work of adhesion as their surface free energy and dispersive and polar components are similar to raw flax fibres, the more polar character of XG counterbalancing the increased dispersive character of CNC modified fibres.

Our results show that the surface treatment of flax fibres with nano-objects as CNC can improve their work of adhesion with mainly apolar matrices such as PP and MAPP thanks to a better polar / dispersive balance at the fibre surface. The use of PP based coupling agents functionalized with maleic anhydride groups (MAPP) allows a further increase of the work of adhesion due to their higher surface tension and polarity providing that MAPP efficiently migrates to the fibre / PP interfaces.

3.2. Crystallization and microstructure of biocomposites

3.2.1. Crystallization of PP and PP / MAPP

DSC analyses were performed to study the effect of the adsorption of CNC and XG/CNC on flax fibres on the crystallization of PP and PP / MAPP. In fact, the chemical composition as well as the topography of fibre surfaces could play a role on the crystallization behaviour of polymer matrices (Girones, Vo, Haudin, Freire, & Navard, 2017; Wang, Tong, Hou, Li, & Shen, 2011). Curves of the first heating scan and cooling scan are represented in Fig. 1S of the supplementary data file for each prepared biocomposite. First, melting temperatures T_m of the different biocomposites were similar, i.e. roughly 166–170 °C, indicating that the presence of CNC and XG/CNC on flax fibre surfaces did not significantly affect the melting and hence the structure of PP crystals formed.

Crystallization temperatures T_c were measured during the cooling step and showed slight differences between biocomposites as shown in Table 3. PP_flax, PP_flax_CNC and PP_MAPP_flax had T_c = 131–132 °C, while PP_MAPP_flax_CNC and PP_MAPP_flax_XG/CNC display lower T_c around 127 °C. It seems that the combination of both MAPP and CNC (or XG/CNC) induces a change in the crystallization behaviour of PP with a slight decrease of its crystallization temperature, and hence a possible delayed and/or reduced nucleation. Further isothermal crystallization analysis by DSC and polarized optical microscopy observations would be

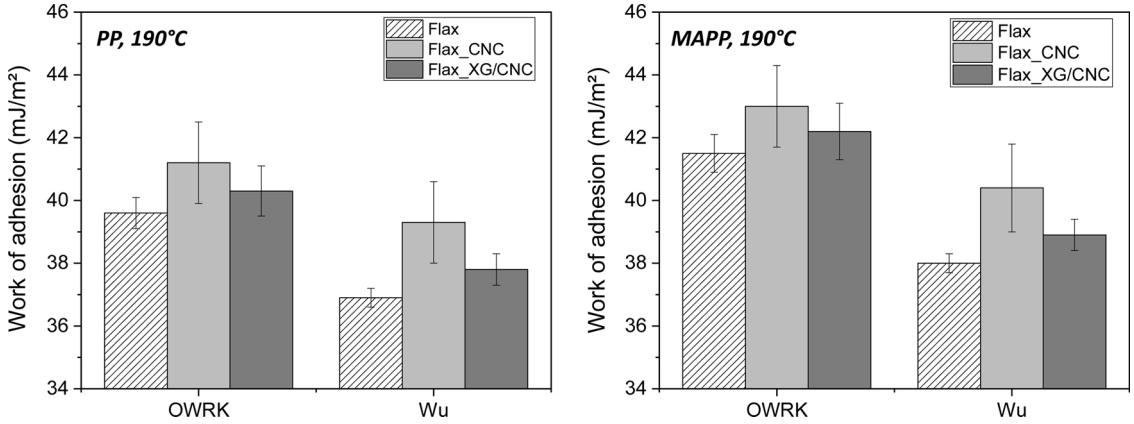

Fig. 1. Work of adhesion between non-treated or treated flax fibres, and PP or MAPP matrices at 190 °C calculated by OWRK (Eq. 4) and Wu (Eq. 5) approaches.

Table 3
Melting temperature T_m and enthalpy ΔH_m, degree of crystallinity X_c and crystallization temperature T_c of the matrix determined from the first heating and cooling scans of DSC thermograms for PP or PP / MAPP based biocomposites reinforced with 20 wt% flax fibres (non-treated, CNC and XG/CNC treated).

	Melting temperature T_m (°C)	Melting enthalpy ΔH_m (J/g)	Degree of crystallinity χ_c (%)	Crystallization temperature T_c (°C)
PP_flax	168.2 ± 1.1	61.9 ± 0.6	37.3 ± 0.4	132.4 ± 0.1
PP_flax_CNC	168.9 ± 0.3	62.1 ± 0.0	37.5 ± 0.0	132.7 ± 0.4
PP_MAPP_flax	170.3 ± 1.3	62.2 ± 1.4	37.6 ± 0.8	131.1 ± 1.0
PP_MAPP_flax_CNC	165.7 ± 0.2	61.2 ± 0.3	37.0 ± 0.2	127.2 ± 0.1
PP_MAPP_flax_XG/CNC	167.8 ± 2.1	58.8 ± 0.1	35.5 ± 0.1	126.8 ± 0.4

necessary to better depict the effect of flax fibres a nd t heir surface modification on the crystallization behaviour of PP.

PP / MAPP based biocomposites reinforced with XG/CNC modified flax fibres also showed a slight decrease in the degree of crystallinity X_c from around 37.5 % to 35.5 % (Table 3). This can be explained by the occurrence of covalent bonds between MAPP and the hydroxyl groups present at the surface of XG/CNC assemblies. This leads to the formation of a covalent bond network of lower molecular mobility at the fibres / matrix interface that could locally hamper the crystallization of PP matrix. This phenomenon is also likely to occur with non-treated flax fibres but the higher specific surface area of CNC implies a higher amount of available hydroxyl groups at the surface of fibres, and hence possibly more covalent bonds with MAPP.

3.2.2. *Fibre size and shape distribution*

The fibre treatments could affect the fibre size and shape distribution within the biocomposites after extrusion and injection processes, so microstructural analysis was performed to investigate this possible effect. In fact, changes in fibre morphology influence greatly the mechanical properties of composite materials. In particular, the higher the aspect ratio, the most efficient is the load transfer from the matrix to the fibres, and the higher is the stiffness and strength of the composite.

An example of 4 mm x 4 mm cartography obtained by SEM on the polished surfaces of tensile specimens is shown in Fig. 2a. All cartographies of each biocomposite polished surface are shown in Fig. 2S in the supplementary data file. A good dispersion and individualization into elementary fibres is observed for a large fraction of flax fibres for all biocomposites with the presence of small particles and also some fibre bundles having much higher diameters. Results of the fibre aspect ratio distributions weighted in number and surface are reported in Fig. 2b. Median aspect ratios are very similar for the two weighted distributions and for all biocomposites. They are ranged from 2.9 to 3.2 and from 3.4 to 3.8 for number and surface weighted distributions, respectively. This indicates that the morphology of flax fibres after biocomposite processing was not affected by the different treatments, i.e. addition of MAPP coupling agent and adsorption of CNC or XG/CNC. The obtained mechanical properties of the biocomposites should thus not be influenced by variations in fibre aspect ratio.

Concluding, fibre modifications and MAPP coupling agent did not induce any significant variations in the biocomposite microstructure in terms of fibre size and shape distributions and matrix crystallinity. We thus postulate that the mechanical behaviour of the biocomposites should primarily be influenced by variations in the interfacial adhesion brought by the treatments with CNC and XG/CNC on the flax fibre surface.

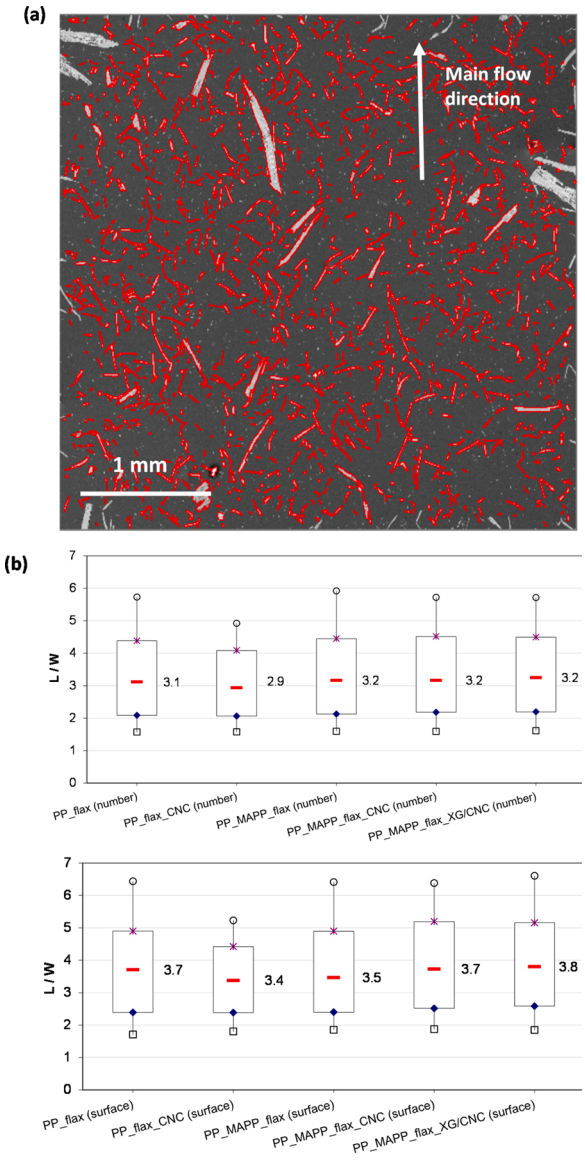

Fig. 2. (a) An example of 4 mm x 4 mm cartography obtained by SEM for the PP_flax biocomposite. Red lines correspond to automatic detection of the outlines of flax fibres further used for image analysis, (b) resulting box-plots of fibre aspect ratio distributions weighted in number and in surface for the different biocomposites (For interpretation of the references to colour in this figure legend, the reader is referred to the web version of this article).

3.3. *Mechanical behaviour and interfacial adhesion of biocomposites*

Previously, CNC adsorption onto flax fibres has been shown to lead to better work of adhesion with the matrix, this being primarily due to increased dispersive character of the fibre surface. Moreover, the MAPP coupling agent also increases the work of adhesion thanks to its higher surface tension and polarity. Macro- and micro-mechanical tests were conducted to study the influence of the combination of the MAPP coupling agent and CNC or XG/CNC fibre treatments on the mechanical behaviour and interfacial adhesion in biocomposites at different length scales.

3.3.1. *Uniaxial tensile tests*

Uniaxial tensile tests were perfomed on biocomposites to determinate their Young's moudulus E as well as their tensile strength σ_{max} and work of rupture, which are more sensitive to failure mechanisms at the fibre / matrix interface and hence interfacial modifications (Le Moigne, Otazaghine, Corn, Angellier-Coussy, & Bergeret, 2018). The results of the uniaxial tensile tests are presented in Fig. 3.

As expected, Young's modulus (Fig. 3c) increases with the amount of flax fibres (Puch & Hopmann, 2015). No pronounced effects of the CNC and XG/CNC fibre functionalization were observed as the Young's modulus is generally little influenced by the interfacial adhesion, especially for short natural fibre composites for which the quantity of fibre / matrix interfaces developed is limited (Le Moigne et al., 2018, Agarwal, Broutman, & Chandrashekhara., 2017). We can also observe that the presence of the MAPP coupling agent even slightly decreases the Young's moduli of the biocomposites. It could be explained by a plasticizing effect related to the presence of MAPP within the bulk of the PP matrix that did not migrate to the fibre / matrix interface.

In contrast, pronounced variations in tensile strength (Fig. 3b) are observed for the different biocomposites depending on the interfacial modifications, either MAPP coupling agent, CNC, or XG/CNC fibre functionalizations. Without the presence of MAPP, it is obvious that the PP / flax interface is not cohesive. The increase in fibre content even results in a slight decrease of the tensile strength because of this weak interfacial adhesion. The same trend is observed for raw flax and

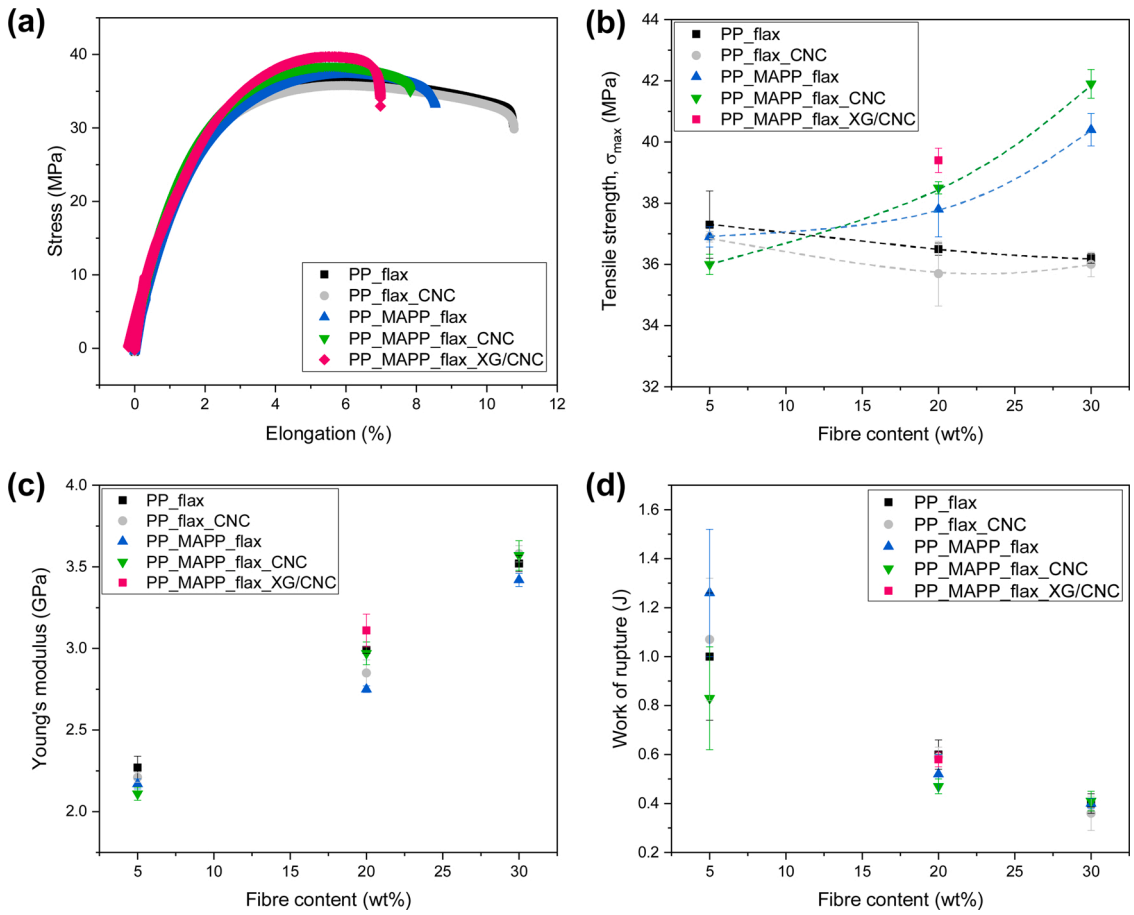

Fig. 3. Typical uniaxial tensile curves at 20 wt% fibre content (a), tensile strength (b), Young's modulus (c) and work of rupture (d) for the different biocomposites.

flax_CNC fibres. On the other hand, the incorporation of MAPP appears to increase the tensile strength, especially for the highest flax fibre contents. For 30 wt% flax fibres, the tensile strength increases significantly from 36.2 ± 0.2 MPa 40.4 ± 0.5 MPa for respectively PP_ flax and PP_MAPP_flax (p-value = 0.0079 based on the statistical Mann & Whitney non-parametric U test). The novelty of our approach is the combination of MAPP with the flax fibre treatment by CNC and XG/CNC. The presence of CNC and XG/CNC on fibre surfaces has a positive effect on the tensile strength of the biocomposite. In fact, the tensile strength increases from 37.4 ± 0.9 MPa 38.5 ± 0.2MPa and 39.3 ± 0.3 MPa for respectively PP_MAPP_flax, PP_MAPP_flax_CNC and PP_MAPP_flax_XG/CNC at 20 wt% flax fibres (p-values of 0.19 and 0.015, respectively, based on the statistical Mann & Whitney non-parametric U test). This shows that the combination of CNC or XG/CNC functionalizations onto flax fibres combined with the incorporation of MAPP coupling agent improves the interfacial adhesion, possibly due to increased interfacial area and preferential chemical interactions between CNC and MAPP.

The work of rupture (Fig. 3d) decreases significantly with increasing fibre content. In fact, the incorporation of flax fibres makes

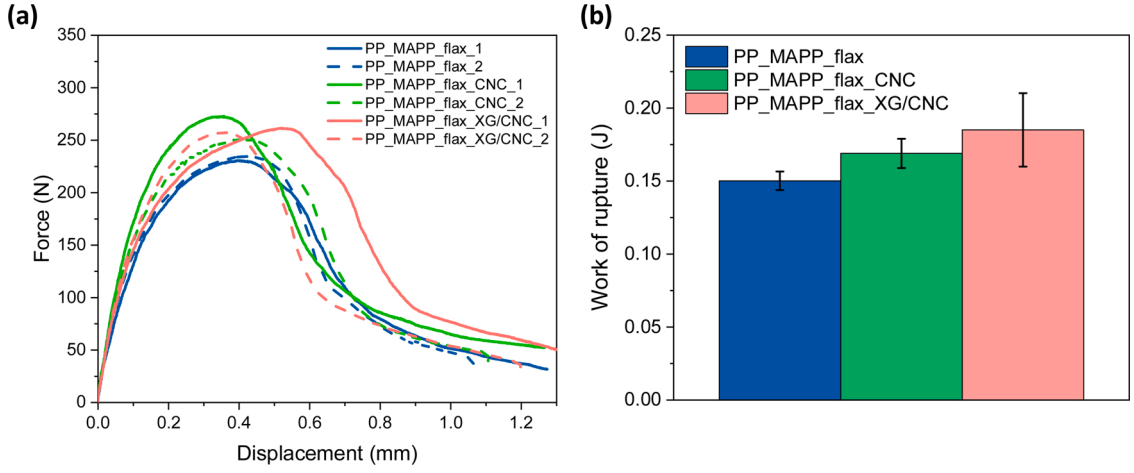

Fig. 4. (a) Force - displacement curves recorded during the micro-tensile test for two notched specimens of PP_MAPP_flax, PP_MAPP_flax_CNC and PP_MAPP_flax_XG/CNC with 20 wt% flax fibres and (b) the resulting work of rupture.

biocomposite materials less ductile with much lower elongation at break as seen on Fig. 3a. The increase in tensile strength brought by interfacial modifications cannot compensate for this loss in ductility, thereby leading to a decreased work of rupture.

3.3.2. *Micro-mechanical tensile tests*

The developed *in situ* micro-mechanical tensile SEM test allows direct observations of crack propagation while recording force-displacement curves (Fig. 4a). This experiment could be assimilated to a pull-out test at a larger scale, i.e. several fibres and bundles are progressively extracted from the matrix during the test. These experiments were performed to better depict the effect of CNC and XG/CNC treatments on interfacial adhesion of flax / PP at the microscale. First, the PP_MAPP_flax composites break at average 233 ± 2 N, while PP_MAPP_flax_CNC and PP_MAPP_flax_XG/CNC break at higher tensile forces, respectively 262 ± 15 N and 260 ± 3 N. The strength improvement related to interfacial adhesion is thus more pronounced with the micro-mechanical tensile test, which is conducted at low tensile speed (0.1 mm/min), especially for matrices showing a strong strain rate dependency as PP (Caro et al., 2018). Besides, the quality of interfacial adhesion and its role on composite failure could also be strain rate dependent. In this regard, it was found that the relation between interfacial adhesion and impact toughness of PP / glass particles systems became less pronounced as strain rate was increased (Thio, Argon, & Cohen, 2004). Nevertheless, the authors could not conclude on the origin of this strain rate dependency, being either related to the interfacial failure mechanism itself or to the plastic strain characteristics of the polymer matrix.

Moreover, the work of rupture during crack propagation has been calculated (Fig. 4b). The biocomposites with CNC and XG/CNC modified flax fibres have higher work of rupture with an increase of 12.5 % and 21.6 %, respectively. This suggests that the presence of both XG and CNC on the flax fibres modifies the failure mechanisms in the interphase zone between fibres and matrix, leading to higher forces and elongation at break. This extensible XG/CNC network with strong interactions and increasing rupture distance was characterized in our previous work (Doineau et al., 2020) by AFM adhesive force measurements. Our results suggest that such a network can have a positive influence on the breaking strength of composite systems.

An analysis of the failure mechanisms by *in situ* visualization of the crack propagation has been conducted for the different biocomposites (Fig. 5 **and Videos 1, 2 and 3**). As regards the local fibre / matrix interfacial adhesion, behaviours are similar and characteristic of both adhesive and cohesive interfacial failures. Indeed, fibre debonding as well as fibre breakage occurs, the matrix showing mainly ductile behaviour with stretching and tearing. Nevertheless, flax fibres modified by CNC and XG/CNC change the failure pattern of the biocomposites. In the case of PP_MAPP_flax, the failure occured through the formation of a macro-crack that propagated quasi-linearly behind the crack tip. In contrast, the crack propagation in PP_MAPP_flax_CNC and PP_MAPP_flax_XG/CNC was more uneven and occured through the formation of numerous micro-cracks. These qualitative observations support the higher work of rupture measured for these biocomposites.

The modification of interphases by the development of hierarchical natural fibres with biopolymers and nano-reinforcements such as XG/CNC thus appears as an interesting strategy to modify failure mechanisms and enhance the strength of biocomposite materials. However, it appears that a chemical coupling between the matrix and modified flax fibres such as MAPP is needed to ensure good interfacial strength and hence better work of rupture.

3.3.3. *Work of adhesion versus practical adhesion*

Fig. 6 shows the correspondence between the work of adhesion that is only governed by physico-chemical interactions between the fibres and the matrix; and the practical adhesion that is related to interfacial strength and influenced by fibre / matrix chemical interactions, mechanical anchorage, transcrystallinity at the interphase and intra and intercellular cohesion within elementary flax fibres and bundles (Le Moigne et al., 2018).

Both plots provide evidence that the combination of interfacial modifications with (i) MAPP coupling agent that brought covalent bonds with the fibres and; (ii) hierarchical fibres functionalized by CNC or XG/CNC assemblies that modify the mechanical behaviour in the interphase zone, could improve the ultimate properties of biocomposites with higher tensile strength and more progressive local failure with higher work of rupture.

4. Conclusions

The interphase of PP / short flax fibre thermoplastic composites was modified by the combination of two strategies, i.e. (i) chemical coupling by MAPP and (ii) flax fibre nanostructuration with the adsorption of CNC and XG. The resulting fibres and biocomposites were characterized by wettability tests, microstructural analysis, micro-mechanical tensile tests with *in situ* SEM observations and uniaxial tensile tests. The presence of cellulose nanocrystals on the surface of flax fibres decreased their polar character and improved the work of adhesion with PP / MAPP matrix. Uniaxial tensile tests revealed that combining the incorporation of MAPP coupling agent and the adsorption of CNC or XG/CNC on flax fibres enhanced the strength of PP / flax biocomposites. Furthermore, the work of rupture of the materials measured by micro-mechanical tensile tests was improved by 12.5 % and 21.6 % for CNC and XG/CNC treatments, respectively. To conclude, the combination of interfacial modifications with nanostructured fibres via the adsorption of CNC and XG/CNC at their surface and the use of coupling agent MAPP that provides covalent bonds with fibres, improves the ultimate

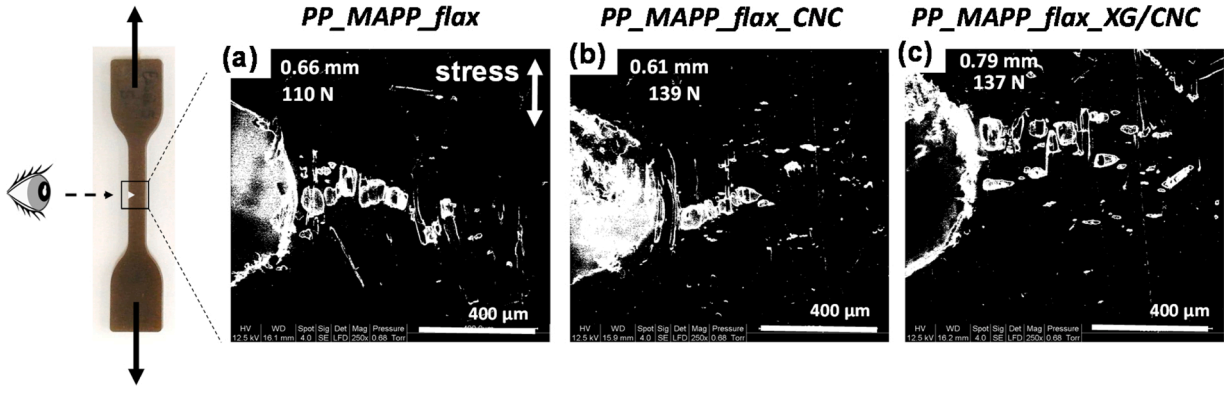

Fig. 5. SEM observations during crack propagation in notched specimens for (a) PP_MAPP_flax, (b) PP_MAPP_flax_CNC and (c) PP_MAPP_flax_XG/CNC with 20 wt% flax fibres. Note that a B&W threshold was applied to the pictures to ease the observation of the described failure phenomena.

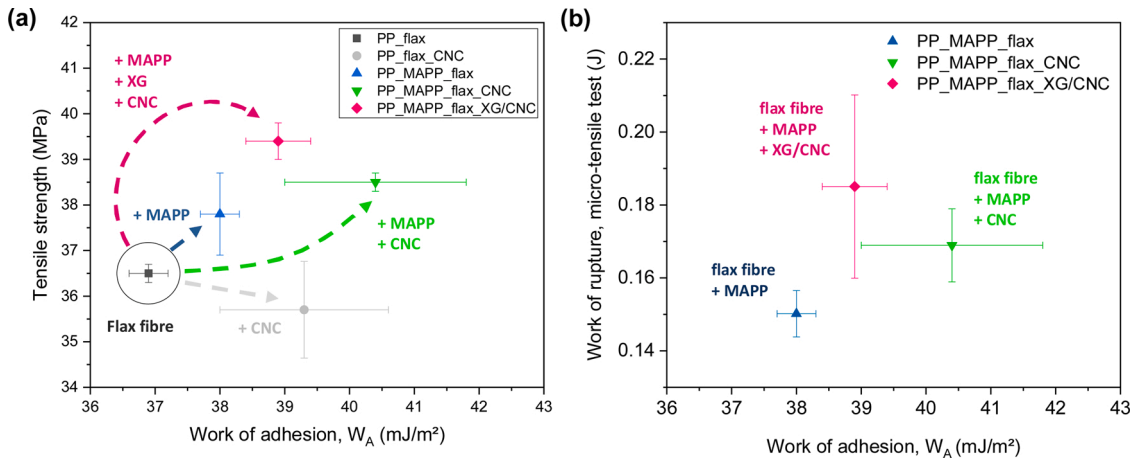

Fig. 6. (a) Tensile strength by uniaxial tensile tests and (b) work of rupture measured by micro-tensile tests for the different biocomposites at 20 wt% flax fibres versus the calculated work of adhesion W_a (Eq. 5) between flax fibres and matrix.

properties of biocomposites, giving higher strength and work of rupture, and more progressive local failures. These results open interesting perspectives for the development of bio-based hierarchical composites with enhanced structural properties, inspired by naturally occurring structures.

CRediT authorship contribution statement

Estelle Doineau: Methodology, Validation, Formal analysis, Investigation, Writing - original draft, Writing - review & editing, Visualization, Funding acquisition. **Guillaume Coqueugniot:** Methodology. **Monica Francesca Pucci:** Methodology, Validation, Writing - review & editing. **Anne-Sophie Caro:** Software, Investigation, Validation, Writing - review & editing. **Bernard Cathala:** Conceptualization, Methodology, Validation, Resources, Writing - review & editing, Supervision, Project administration. **Jean-Charles Bénézet:** Conceptualization, Validation, Writing - review & editing, Supervision, Project administration, Funding acquisition. **Julien Bras:** Conceptualization, Methodology, Validation, Writing - review & editing, Supervision, Project administration. **Nicolas Le Moigne:** Conceptualization, Methodology, Validation, Writing - review & editing, Visualization, Supervision, Project administration, Funding acquisition.

Acknowledgements

Estelle Doineau thanks IMT Mines Alès and Doctoral School GAIA for funding his PhD work. A part of this work was supported by the French research cluster CNRS-INRA' Symbiose' SYnthon et Matériaux BIO-Sourcés for mission funding, and by Glyco@alps (ANR-15-IDEX-02), Idex UGA. LGP2 is part of the LabEx Tec 21 (Investissements d'Avenir – grant agreement n°ANR-11-LABX-0030) and of PolyNat Carnot Institute (Investissements d'Avenir – grant agreement n°ANR-16-CARN-0025-01).

Appendix A. Supplementary data

Supplementary material related to this article can be found, in the online version, at doi:https://doi.org/10.1016/j.carbpol.2020.117403.

References

Abdennadher, A. (2015). *Injection moulding of natural fibre reinforced polypropylene: Process, microstructure and properties*. PhD Thesis. Ecole nationale supérieure des Mines de Paris.

Agarwal, B. D., Broutman, L. J., & Chandrashekhara, K. (2017). *Analysis and performance of Fiber composites*. John Wiley & Sons.

Asadi, A., Miller, M., Singh, A. V., Moon, R. J., & Kalaitzidou, K. (2017). Lightweight sheet molding compound (SMC) composites containing cellulose nanocrystals. *Composite Structures, 160*, 211–219.

Asadi, A., Miller, M., Sultana, S., Moon, R. J., & Kalaitzidou, K. (2016). Introducing cellulose nanocrystals in sheet molding compounds (SMC). *Composites Part A, Applied Science and Manufacturing, 88*, 206–215.

Baley, C., Le Duigou, A., Bourmaud, A., & Davies, P. (2012). Influence of drying on the mechanical behaviour of flax fibres and their unidirectional composites. *Composites Part A, Applied Science and Manufacturing, 43*(8), 1226–1233.

Bay, R. S., & Tucker, C. L., III (1992). Fiber orientation in simple injection moldings. Part I: Theory and numerical methods'. *Polymer Composites, 13*(4), 317–331.

Berzin, F., Lemkhanter, L., Marcuello, C., Chabbert, B., Aguié-Béghin, V., Molinari, M., Castellani, R., & Vergnes, B. (2020). Influence of the polarity of the matrix on the breakage mechanisms of lignocellulosic fibers during twin-screw extrusion. *Polymer Composites, 41*(3), 1106–1117.

Bismarck, A., Aranberri-Askargorta, I., Springer, J., Lampke, T., Wielage, B., Stamboulis, A., Shenderovich, I., & Limbach, H.-H. (2002). Surface characterization of flax, hemp and cellulose fibers; surface properties and the water uptake behavior. *Polymer Composites, 23*(5), 872–894.

Blaine, R. L. (2002). Polymer heats of fusion. *Therm Appl Note TN048, 2002*, 1–2.

Blaker, J. J., Lee, K.-Y., & Bismarck, A. (2011). Hierarchical composites made entirely from renewable resources. *Journal of Biobased Materials and Bioenergy, 5*(1), 1–16.

Bourmaud, J. B., Shah, D. U., Placet, V., & Baley, C. (2018). Towards the design of high-performance plant fibre composites. *Progress in Materials Science, 97*, 347–408.

Caro, A. S., Bernardeau, F., Perrin, D., Leger, R., Benezet, J. C., & Ienny, P. (2018). Computational modelling of void growth in phenolic molding compounds filled PolyPropylene from optical measurements. *Polymer Testing, 71*, 209–216.

Cerclier, C., Guyomard-Lack, A., Moreau, C., Cousin, F., Beury, N., Bonnin, E., Jean, B., & Cathala, B. (2011). Coloured semi-reflective thin films for biomass-hydrolyzing enzyme detection. *Advanced Materials, 23*(33), 3791–3795.

Cerclier, C. V., Guyomard-Lack, A., Cousin, F., Jean, B., Bonnin, E., Cathala, B., et al. (2013). Xyloglucan–Cellulose nanocrystal multilayered films: Effect of film architecture on enzymatic hydrolysis. *Biomacromolecules, 14*(10), 3599–3609.

Dai, D., & Fan, M. (2013). Green modification of natural fibres with nanocellulose. *RSC Advances, 3*(14), 4659.

Daniel Wagner, H. (2002). Nanotube–Polymer adhesion: A mechanics approach. *Chemical Physics Letters, 361*(1), 57–61.

Doineau, E., Bauer, G., Ensenlaz, L., Novales, B., Sillard, C., Bénézet, J.-C., Bras, J., Cathala, B., & Le Moigne, N. (2020). Adsorption of xyloglucan and cellulose nanocrystals on natural fibres for the creation of hierarchically structured fibres. *Carbohydrate Polymers, 248*, Article 116713.

Dufresne, A. (2017). *Nanocellulose: From nature to high performance tailored materials*. Walter de Gruyter GmbH & Co KG.

Elsabbagh, A., Steuernagel, L., & Ziegmann, G. (2009). Effect of fiber/matrix chemical modification on the mechanical properties and water absorption of extruded Flax/Polypropylene composite. *Journal of Applied Polymer Science, 111*(5), 2279–2289.

Faruk, O., Bledzki, A. K., Fink, H.-P., & Sain, M. (2012). Biocomposites reinforced with natural fibers: 2000–2010. *Progress in Polymer Science, 37*(11), 1552–1596.

Fortea-Verdejo, M., Lee, K.-Y., Zimmermann, T., & Bismarck, A. (2016). Upgrading flax nonwovens: Nanocellulose as Binder to produce rigid and robust flax fibre preforms. *Composites Part A, Applied Science and Manufacturing, 83*(Supplement C), 63–71.

Foster, E., Johan, Moon, R. J., Agarwal, U. P., Bortner, M. J., Bras, J., Camarero-Espinosa, S., Chan, K. J., Clift, M. J. D., Cranston, E. D., Eichhorn, S. J., Fox, D. M., Hamad, W. Y., Heux, L., Jean, B., Korey, M., Nieh, W., Ong, K. J., Reid, M. S., Renneckar, S., Roberts, R., Jo, A. S., Simonsen, J., Stinson-Bagby, K., Wanasekara, N., & Youngblood, J. (2018). Current characterization methods for cellulose nanomaterials. *Chemical Society Reviews, 47*(8), 2609–2679.

Fuentes, C. A., Zhang, Y., Guo, H., Woigk, W., Masania, K., Dransfeld, C., De Coninck, J., Dupont-Gillain, C., Seveno, D., & Van Vuure, A. W. (2018). Predicting the adhesion

strength of Thermoplastic/Glass interfaces from wetting measurements. *Colloids and Surfaces A, Physicochemical and Engineering Aspects, 558*, 280–290.
Gao, H., Ji, B., Jager, I. L., Arzt, E., & Fratzl, P. (2003). Materials become insensitive to flaws at nanoscale: Lessons from nature. *Proceedings of the National Academy of Sciences, 100*(10), 5597–5600.
Garat, W., Le Moigne, N., Corn, S., Beaugrand, J., & Bergeret, A. (2020). Swelling of natural fibre bundles under hygro- and hydrothermal conditions: Determination of hydric expansion coefficients by automated laser scanning. *Composites Part A, Applied Science and Manufacturing, 131*, Article 105803.
Ghasemi, S., Tajvidi, M., Bousfield, D. W., & Gardner, D. J. (2018). Reinforcement of natural fiber yarns by cellulose nanomaterials: A multi-scale study. *Industrial Crops and Products, 111*, 471–481.
Girones, J., Vo, L. T. T., Haudin, J.-M., Freire, L., & Navard, P. (2017). Crystallization of polypropylene in the presence of biomass-based fillers of different compositions. *Polymer, 127*, 220–231.
Gupta, H. S., Seto, J., Wagermaier, W., Zaslansky, P., Boesecke, P., & Fratzl, P. (2006). Cooperative deformation of mineral and collagen in bone at the nanoscale. *Proceedings of the National Academy of Sciences, 103*(47), 17741–17746.
Hajlane, A., Joffe, R., & Kaddami, H. (2018). Cellulose nanocrystal deposition onto regenerated cellulose fibres: Effect on moisture absorption and fibre–Matrix adhesion. *Cellulose, 25*(3), 1783–1793.
Hajlane, A., Kaddami, H., & Joffe, R. (2017). Chemical modification of regenerated cellulose fibres by cellulose nano-crystals: Towards hierarchical structure for structural composites reinforcement. *Industrial Crops and Products, 100*, 41–50.
Hughes, J. D. H., Morley, H., & Jackson, E. E. (1980). Aligned carbon fibre composite which approaches theoretical strength. *Journal of Physics D: Applied Physics, 13*(6), 921–936.
Jaafar, Z., Quelennec, B., Moreau, C., Lourdin, D., Maigret, J. E., Pontoire, B., D'orlando, A., Coradin, T., Duchemin, B., Fernandes, F. M., & Cathala, B. (2020). Plant cell wall inspired xyloglucan/cellulose nanocrystals aerogels produced by freeze-casting. *Carbohydrate Polymers, 247*, Article 116642.
Jean, B., Heux, L., Dubreuil, F., Chambat, G., & Cousin, F. (2009). Non-electrostatic building of biomimetic cellulose–Xyloglucan multilayers. *Langmuir, 25*(7), 3920–3923.
Juntaro, J., Pommet, M., Mantalaris, A., Shaffer, M., & Bismarck, A. (2007). Nanocellulose enhanced interfaces in truly green unidirectional fibre reinforced composites. *Composite Interfaces, 14*(7–9), 753–762.
Juntaro, J., Pommet, M., Kalinka, G., Mantalaris, A., Shaffer, M. S. P., & Bismarck, A. (2008). Creating hierarchical structures in renewable composites by attaching bacterial cellulose onto sisal fibers. *Advanced Materials, 20*(16), 3122–3126.
Karger-Kocsis, J., Mahmood, H., & Pegoretti, A. (2015). Recent advances in Fiber/Matrix interphase engineering for polymer composites. *Progress in Materials Science, 73*, 1–43.
Karger-Kocsis, J., Mahmood, H., & Pegoretti, A. (2020). All-carbon multi-scale and hierarchical fibers and related structural composites: A review. *Composites Science and Technology, 186*, Article 107932.
Khaldi, M., Bouziane, M. M., Vivet, A., & Bougherara, H. (2019). About the influence of temperature and environmental relative humidity on the longitudinal and transverse mechanical properties of elementary alfa fibers. *Journal of Applied Polymer Science*, 1–9.
Khoshkava, V., & Kamal, M. R. (2013). Effect of surface energy on dispersion and mechanical properties of Polymer/Nanocrystalline cellulose nanocomposites. *Biomacromolecules, 14*(9), 3155–3163.
Klemm, D., Kramer, F., Moritz, S., Lindström, T., Ankerfors, M., Gray, D., et al. (2011). Nanocelluloses: A new family of nature-based materials. *Angewandte Chemie International Edition, 50*(24), 5438–5466.
Kwok, D. Y., Cheung, L. K., Park, C. B., & Neumann, A. W. (1998). Study on the surface tensions of polymer melts using axisymmetric drop shape analysis. *Polymer Engineering and Science, 38*(5), 757–764.
Lau, K.-T., Hung, P.-Y., Zhu, M.-H., & Hui, D. (2018). Properties of natural fibre composites for structural engineering applications. *Composites Part B Engineering, 136*, 222–233.
Le Duigou, A., Bourmaud, A., Balnois, E., Davies, P., & Baley, C. (2012). Improving the interfacial properties between flax fibres and PLLA by a water fibre treatment and drying cycle. *Industrial Crops and Products, 39*, 31–39.
Le Duigou, A., Kervoelen, A., Le Grand, A., Nardin, M., & Baley, C. (2014). Interfacial properties of flax fibre–Epoxy resin systems: Existence of a complex interphase. *Composites Science and Technology, 100*, 152–157.
Le Duigou, A., Merotte, J., Bourmaud, A., Davies, P., Belhouli, K., & Baley, C. (2017). Hygroscopic expansion: A key point to describe natural fibre/polymer matrix interface bond strength. *Composites Science and Technology, 151*, 228–233.
Le Moigne, N., Otazaghine, B., Corn, S., Angellier-Coussy, H., & Bergeret, A. (2018). *Surfaces and interfaces in natural fibre reinforced composites*. Cham: Springer International Publishing.
Le Moigne, N., van Den Oever, M., & Budtova, T. (2011). A statistical analysis of fibre size and shape distribution after compounding in composites reinforced by natural fibres. *Composites Part A, Applied Science and Manufacturing, 42*(10), 1542–1550.
Lee, K.-Y., Bharadia, P., Blaker, J. J., & Bismarck, A. (2012). Short sisal fibre reinforced bacterial cellulose polylactide nanocomposites using hairy sisal fibres as reinforcement. *Composites Part A, Applied Science and Manufacturing, 43*(11), 2065–2074.
Lee, K.-Y., Delille, A., & Bismarck, A. (2011). Greener surface treatments of natural fibres for the production of renewable composite materials. In S. Kalia, B. S. Kaith, & I. Kaur (Eds.), *Cellulose fibers: Bio- and nano-polymer composites* (pp. 155–178). Berlin, Heidelberg: Springer Berlin Heidelberg.
Li, S., Li, H., Wang, X., Song, Y., Liu, Y., Jiang, L., et al. (2002). Super-hydrophobicity of large-area honeycomb-like aligned carbon nanotubes. *The Journal of Physical Chemistry B, 106*(36), 9274–9276.
Liotier, P.-J., Pucci, M. F., Duigou, A. L., Kervoelen, A., Tirilló, J., Sarasini, F., et al. (2019). Role of interface formation versus fibres properties in the mechanical behaviour of bio-based composites manufactured by liquid composite molding processes. *Composites Part B Engineering, 163*, 86–95.
Lu, J. Z. (2000). Chemical coupling in wood Fiber and polymer composites: A review of coupling agents and treatments. *Wood and Fiber Science, 32*(1), 88–104.
Mohanty, Misra, M., & Drzal, L. T. (2001). Surface modifications of natural fibers and performance of the resulting biocomposites: An overview. *Composite Interfaces, 8*(5), 313–343.
Mohanty, S., Nayak, S. K., Verma, S. K., & Tripathy, S. S. (2016). Effect of MAPP as a coupling agent on the performance of jute–PP composites. *Journal of Reinforced Plastics and Composites*.
Mohanty, S. V., Pin, J.-M., & Misra, M. (2018). Composites from renewable and sustainable resources: Challenges and innovations. *Science, 362*(6414), 536–542.
Moon, R. J., Martini, A., Nairn, J., Simonsen, J., & Youngblood, J. (2011). Cellulose nanomaterials review: Structure, properties and nanocomposites. *Chemical Society Reviews, 40*(7), 3941–3994.
Müssig, J. (2010). *Industrial applications of natural fibres: Structure, properties and technical applications*. John Wiley & Sons.
Owens, D. K., & Wendt, R. C. (1969). Estimation of the surface free energy of polymers. *Journal of Applied Polymer Science, 13*(8), 1741–1747.
Park, J.-M., Quang, S. T., Hwang, B.-S., & Lawrence DeVries, K. (2006). Interfacial evaluation of modified jute and hemp Fibers/Polypropylene (PP)-Maleic anhydride polypropylene copolymers (PP-MAPP) composites using micromechanical technique and nondestructive acoustic emission. *Composites Science and Technology, 66*(15), 2686–2699.
Pickering, K. L., Aruan Efendy, M. G., & Le, T. M. (2016). A review of recent developments in natural fibre composites and their mechanical performance. *Composites Part A, Applied Science and Manufacturing, 83*, 98–112.
Pirich, C. L., Alves de Freitas, R., Woehl, M. A., Picheth, G. F., Petri, D. F. S., & Rita Sierakowski, M. (2015). Bacterial cellulose nanocrystals: Impact of the sulfate content on the interaction with xyloglucan'. *Cellulose, 22*(3), 1773–1787.
Pommet, M., Juntaro, J., Heng, J. Y. Y., Mantalaris, A., Lee, A. F., Wilson, K., Kalinka, G., Shaffer, M. S. P., & Bismarck, A. (2008). Surface modification of natural fibers using Bacteria: Depositing bacterial cellulose onto natural fibers to create hierarchical Fiber reinforced nanocomposites. *Biomacromolecules, 9*(6), 1643–1651.
Pucci, M. F., Liotier, P.-J., Seveno, D., Fuentes, C., Van Vuure, A., & Drapier, S. (2017). Wetting and swelling property modifications of elementary flax fibres and their effects on the liquid composite molding process. *Composites Part A, Applied Science and Manufacturing, 97*, 31–40.
Puch, F., & Hopmann, C. (2015). Experimental investigation of the influence of the compounding process and the composite composition on the mechanical properties of a short flax Fiber–Reinforced polypropylene composite. *Polymer Composites, 36*(12), 2282–2290.
Qian, H., Bismarck, A., Greenhalgh, E. S., Kalinka, G., & Shaffer, M. S. P. (2008). Hierarchical composites reinforced with carbon nanotube grafted fibers: The potential assessed at the single fiber level. *Chemistry of Materials, 20*(5), 1862–1869.
Saba, N., Jawaid, M., & Asim, M. (2016). Recent advances in nanoclay/Natural fibers hybrid composites. In M. Jawaid, A. E. K. Qaiss, & R. Bouhfid (Eds.), *Nanoclay reinforced polymer composites: Natural fibre/nanoclay hybrid composites, engineering materials* (pp. 1–28). Singapore: Springer.
Sanjay, M. R., Madhu, P., Jawaid, M., Senthamaraikannan, P., Senthil, S., & Pradeep, S. (2018). Characterization and properties of natural Fiber polymer composites: A comprehensive review. *Journal of Cleaner Production, 172*, 566–581.
Schonhorn, H., & Sharpe, L. H. (1965). Surface tension of molten polypropylene. *Journal of Polymer Science Part B: Polymer Letters, 3*(3), 235–237.
Sehaqui, H., Zhou, Q., & Berglund, L. A. (2011). High-porosity aerogels of high specific surface area prepared from nanofibrillated cellulose (NFC). *Composites Science and Technology, 71*(13), 1593–1599.
Sharma, M., Gao, S., Mäder, E., Sharma, H., Yew Wei, L., & Bijwe, J. (2014). Carbon Fiber surfaces and composite interphases. *Composites Science and Technology, 102*, 35–50.
Snijder, M. H. B., & Bos, H. L. (2000). Reinforcement of polypropylene by annual plant fibers: Optimisation of the coupling agent efficiency. *Composite Interfaces, 7*(2), 69–75.
Thio, Y. S., Argon, A. S., & Cohen, R. E. (2004). Role of interfacial adhesion strength on toughening polypropylene with rigid particles. *Polymer, 45*(10), 3139–3147.
Tran, L. Q. N., Fuentes, C. A., Dupont-Gillain, C., Van Vuure, A. W., & Verpoest, I. (2013). Understanding the interfacial compatibility and adhesion of natural coir fibre thermoplastic composites. *Composites Science and Technology, 80*, 23–30.
Wang, Y., Tong, B., Hou, S., Li, M., & Shen, C. (2011). Transcrystallization behavior at the poly(Lactic acid)/Sisal fibre biocomposite interface. *Composites Part A, Applied Science and Manufacturing, 42*(1), 66–74.
Wu, S. (1971). Calculation of interfacial tension in polymer systems. *Journal of Polymer Science Part C Polymer Symposia, 34*(1), 19–30.
Yan, L., Chouw, N., & Jayaraman, K. (2014). Flax fibre and its composites – A review. *Composites Part B Engineering, 56*, 296–317.
Yang, C., Han, R., Nie, M., & Wang, Q. (2020). Interfacial reinforcement mechanism in poly(Lactic acid)/Natural Fiber biocomposites featuring ZnO nanowires at the interface. *Materials & Design, 186*, Article 108332.
Zafeiropoulos, N. E. (2011). *Interface engineering of natural fibre composites for maximum performance*. Elsevier.